minerals

MDPI

Article

Use of Cemented Super-Fine Unclassified Tailings Backfill for Control of Subsidence

Lei Yang [1,2], Jingping Qiu [1,*], Haiqiang Jiang [1], Shiqiang Hu [1], Hao Li [1] and Songbo Li [3]

[1] Key Laboratory of Ministry of Education on Safe Mining of Deep Metal Mines, Northeastern University, Shenyang 110819, China; yanglei_neu@foxmail.com (L.Y.); hqjiang2007@126.com (H.J.); dukenasser419@outlook.com (S.H.); LIHAO2017D@hotmail.com (H.L.)

[2] School of Engineering, RMIT University, Melbourne, VIC 3000, Australia

[3] Faculty of Education, Northeast Normal University, Changchun 130024, China; lisb880@nenu.edu.cn

* Correspondence: qiujingping@mail.neu.edu.cn; Tel.: +86-024-8368-6660

Received: 11 October 2017; Accepted: 6 November 2017; Published: 9 November 2017

Abstract: Known for its advantages in preventing geological and environmental hazards, cemented paste backfill (CPB) has become a topic of interest for scientists and mining engineers in recent decades. This paper presents the results of a study on the use of cemented super-fine tailings backfill (CSUTB) in an underground mine for control of surface subsidence. An analytical solution is developed based on the available model to calculate the required strength of backfill when in contact with non-cemented tailings (NCT). The effect of solid contents on the rheological properties of CSUTB is investigated. A reasonable mix proportion (RMP) of CSUTB is determined for Zhongguan Iron Mine (ZGIM) based on laboratory experiments. The validity of RMP in surface subsidence control is verified by a 3D numerical model. The obtained results show that CSUTB requires higher strength when in contact with NCT than when in contact with orebody. Rheological characteristics, e.g., slump, fluidity, and bleeding rate of fresh CSUTB, decrease with higher solids content, of which values with a certain solids content can be determined by quadratic polynomial regression equations. RMP with a cement to tailings (c/t) ratio of 1:10 and a solids content of 70% is recommended for ZGIM, as it shows favorable mechanical and rheological abilities. The deformation parameters (curvature, inclination, and horizontal deformation rate) obtained from numerical modeling are acceptable and lower than critical values, meaning CSUTB can feasibly be used with RMP in subsidence control.

Keywords: super-fine tailings; cemented backfill; Mitchell solution; rheological properties; subsidence control

1. Introduction

Underground mining is the primary method to remove and excavate economically valuable minerals, but it usually co-produces a large number of voids and large quantities of waste materials, e.g., tailings and coal gangue. Underground voids often lead to stope instability and ground subsidence, causing damage to residential buildings and infrastructures [1,2]. In China, the subsidence area caused by mining activity has reached 314,765 km^2, resulting in 535 deaths and economic losses of $1.9 billion [3]. Meanwhile, massive tailings generated from mineral processing have been deposited into more than 3000 tailings dams (ponds) without any further steps due to its low cost [4,5]. However, this method of disposal entails geological (e.g., tailings dam failures) and environmental (e.g., acid mine drainage, heavy metal leaching and groundwater pollution) hazards [6–8]. For example, a tailings dam located in Shanxi province, China collapsed in 2008, causing 277 casualties and direct economic losses of $14.59 million. More seriously, the quantity of tailings in China is still increasing at a speed of 600 million tons per year [3].

A typical way to treat and prevent the aforementioned hazards is known as backfill technology, which fills the underground gob with CPB [9]. CPB has become one of the most important mining

methods, after being first used in Bad Grund Mine in Germany in the late 1970s, as it can (a) prevent surface subsidence, (b) dispose of solid waste as a tailings storage area, (c) reduce ore dilution and mining cycles, and (d) improve the working environment [4,10–14]. Meanwhile, CPB has lower operating costs and higher strength acquisition compared with other backfill technologies including cemented rock fill and hydraulic backfill [15]. CPB, with solid content between 70% and 85%, is a mixture of water, total mill tailings, and binder (e.g., cement, fly ash, or blast furnace slag) to reach the desired strength and rheology.

Treatment and utilization of super-fine tailings (SFT) has always been an interesting research topic due to safety and environmental problems. Compared with coarse tailings, SFT involves slow-settling, unreasonable particle size distribution and special chemical composition [16]. Few studies have been conducted to evaluate the effect of fine tailings on the quality of CPB. Amaratunga et al. [17] found that the strength and elastic modulus of paste fill increased significantly when fine tailings were added as agglomerate pellets. Kesimal et al. [18] observed that decreasing the fines contents via desliming had a positive effect on UCS of backfill. Fall et al. [19] firstly investigated the influence of tailings particle size on the properties of hardened CPB (e.g., strength, cost and microstructure) and fresh CPB (e.g., water demand). They reported that an increase in finer particles led to lower strength, poor workability, and higher moisture content and water demand, which is consistent with the findings in [13]. Ke et al. [20] also concluded that fine tailings positively affected the critical pore diameter and numbers in CPB. However, super-fine tailings' properties, e.g., chemical, physical, and mineralogical characteristics, are variable with geological conditions (e.g., rock properties and ore mineralogy) and physical and chemical process of extraction [7], leading to different qualities of CPB (CSUTB in this study).

For the use of backfill in subsidence control, a number of studies have reported using analytical solutions, physical models, and numerical modeling. Siriwardane et al. [21] concluded that fluidized-bed combustion ash could be used as an engineering material in coal mines to control surface subsidence, which was clearly influenced by backfill ratio. Zhu et al. [22] also insisted that filling ratio and porosity of backfill material had an obvious effect on surface subsidence by using a coupled discrete element-finite difference method. Zhang et al. [23] and Guo et al. [24] proposed analytical models for predicting surface subsidence in solid backfill mining based on the equivalent mining height theory. Sui et al. [25] evaluated the subsidence of Taiping Coal mine based on numerical simulation and a scale model and noted that subsidence could be mitigated by the backfilling method so as to prevent sand and water inrushes. Application of CPB in metal mine has also been investigated by a few researchers. Huang et al. [26] investigated the surface subsidence of Luohe Iron mine based on a 3D discontinuum numerical model and found that backfill significantly reduced subsidence and the distribution of subsidence was associated with orebody geometry. Yang et al. [27] investigated the backfill stability and subsidence distribution in Sijiaying Iron Mine by combining numerical modeling and a physical model. However, reports about the application of CSUTB in subsidence control are scarce.

Owing to concerns about ground villages and stricter environmental regulations in China, backfilling technology is also used in ZGIM. UCS of CSUTB of ZGIM at given times has been successfully investigated in a previous study [28], whereas the rheological properties of CSUTB are not clear. Meanwhile, a reasonable mix proportion (RMP) of backfill for ZGIM needs to be determined to reduce mining costs and meet the strength requirement of mining. Therefore, based on field conditions in ZGIM, the main objectives of this study are as follows:

1. To determine the required strength of CSUTB with an exposure for ZGIM
2. To analyze the effect of solids content on rheological characteristics of fresh CSUTB
3. To determine the RMP of CSUTB for ZGIM
4. To verify the validity of the CSUTB with RMP in surface subsidence control using numerical modeling.

The paper is organized as follows: an introduction of the geological condition and mining sequence of ZGIM is first presented. This is followed by an analytical solution for determining the required strength of backfill in ZGIM. After that, the optimal mix design of CSUTB meeting the strength and transportation requirement is recommended. Then, the mechanical parameters of CSUTB with aforementioned mix design are input into numerical modeling to investigate its validity in subsidence control. Finally, we present our conclusions.

2. Geological and Mining Conditions of ZGIM

As shown in Figure 1, Zhongguan Iron Mine (ZGIM, Hesteel Group Co., Ltd., an underground iron mine) is located at Zhongguan County, Shahe City, 30 and 53 km away from Xingtai and Handan, respectively, Hebei province, China. ZGIM (36°55′ N, 114°01′ E) has a temperate continental monsoon climate with a mean annual rainfall of 544 mm. The orebody strikes NE 10° to 14°, dips to SE with an average dip angle of 46°, and has a buried depth ranging from 300 to 500 m. The overall topography above the mining area is high in the west and low in the east, and ground elevation is in the range of +200 to +270 m. Rotary coring showed that quaternary topsoil, shale, crystalline limestone (hanging wall rock), iron, and marble (footwall rock) are the dominant lithological materials in the mine. A generalized stratigraphic section is shown in Figure 2.

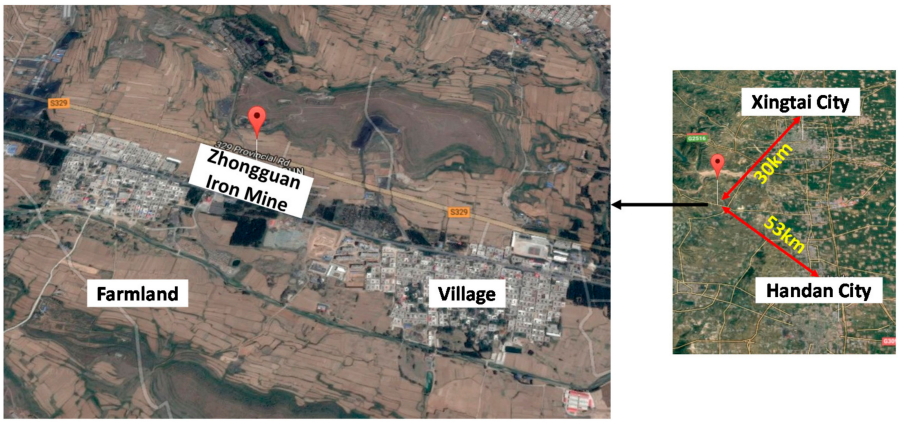

Figure 1. Location of Zhongguan iron mine.

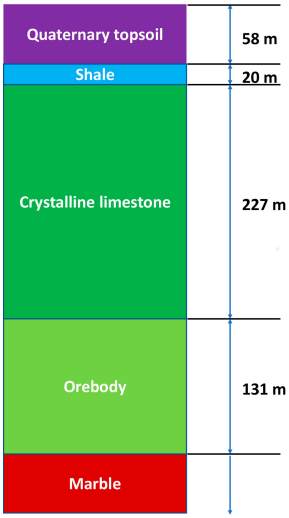

Figure 2. Generalized stratigraphic column at ZGIM.

Considering the strict regulations related to environmental protection in China and to protect surface residential buildings and farmland, as shown in Figure 1, a two-step sublevel open stoping mining method with delayed backfill is used for ZGIM. The whole orebody is divided into five levels at every 60 m, i.e., −110, −170, −230, −290 and −350 m. The panel is arranged along the strike with 114 m length, and separated into primary and secondary stopes. The stope with 18 m width and 50 m length is perpendicular to the strike, and the permanent pillar between the panels is 6 m wide. The primary stope is mined out first, the ore is mucked from draw points after blasting, and then CPB is placed into the stope from the top drift. After three to four months' curing, the secondary stope is extracted and placed with NCT. The mining-backfilling sequence of primary and secondary stopes is shown in Figure 3. The designed mining sequence of levels in ZGIM is as follows: −350 m > −290 m > −230 m > −170 m > −110 m.

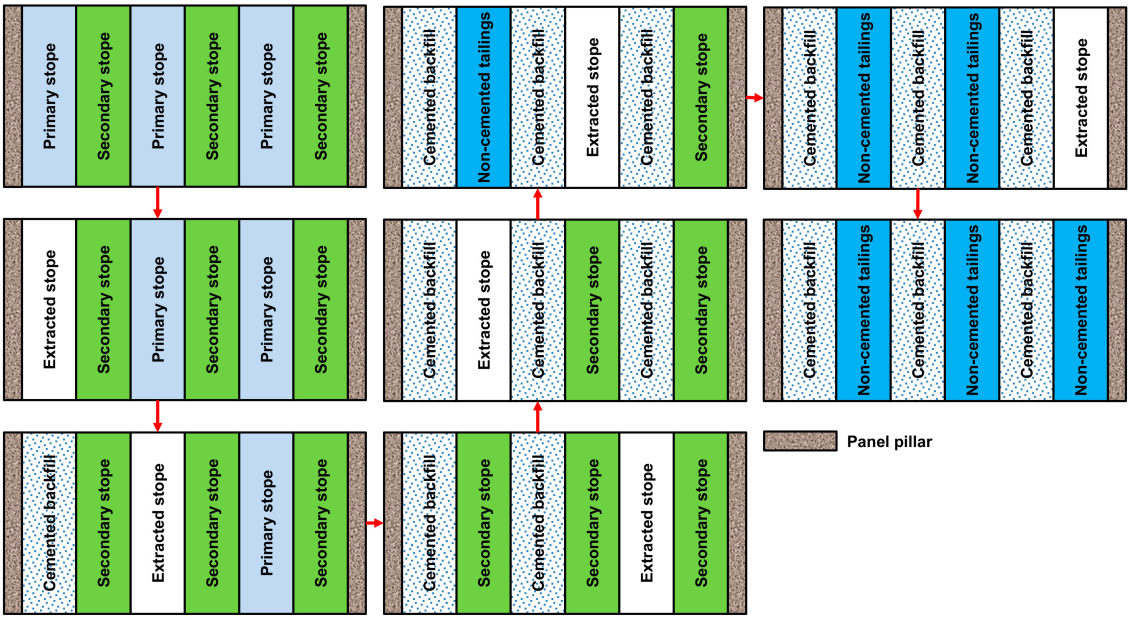

Figure 3. Mining–backfilling sequence of stopes in panel.

3. Required Strength of CSUTB for ZGIM

3.1. Analytical Solution for CSUTB when in Contact with the Orebody

CPB needs an adequate strength to remain self-standing and resist blast disturbance during mining process of secondary stope. In order to calculate the required strength of CPB, a lot of models have been proposed and modified [29–34]. In general, the most widely used model is developed based on Mitchell et al. [35] in 1982 using limit equilibrium analysis. However, this model has several limitations [30]: (a) it considered the cohesion of interfaces between backfill and side wall equal to that of backfill, which is contrary to experimental results obtained from Fall and Nasir [36]; (b) it neglected the shear strength along the interfaces between backfill and side/back wall; and (c) it did not consider the surface load such as miners and equipment. Considering the abovementioned disadvantages, Li and coworkers proposed a modified Mitchell model [29] and a generalized solution [30] for calculating the required strength of backfill with a vertical exposure. The three-dimensional model they used is shown in Figure 3. Fill body tends to slide and move toward the new extracted space after secondary stope extraction, caused by driving forces including block weight and surface load (q). Meanwhile, a critical failure plane (shear sliding plane) will be formulated. To keep fill body stable, cohesion, and particle friction, both in backfill and in interfaces of backfill-orebody/side walls, interfaces would produce shear force along the failure surface to resist shear sliding. In Figure 4, L is

the stope length vertical to the orebody strike; B is the strike width; H is the stope height; τ_s. and τ_a are the shear strengths of the backfill-side wall and backfill-orebody interfaces, respectively; H_1 is the height of wedge block; and α is the angle between the sliding plane and the horizontal plane.

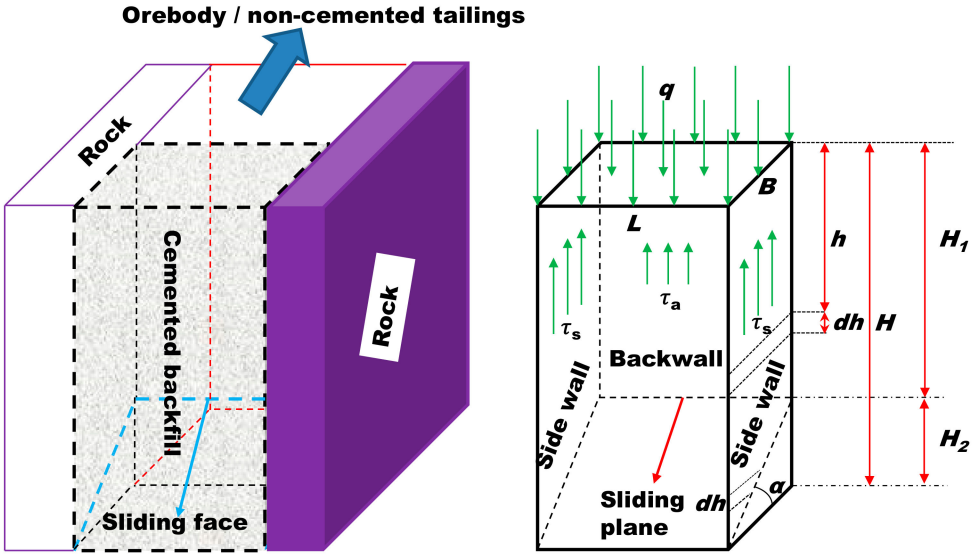

Figure 4. Wedge block model (adapted from [30]).

The required uniaxial compressive strength (UCS) of backfill is expressed as [30]:

$$UCS = \frac{L}{K\tan\delta}\cdot\left\{\gamma - \frac{1}{B\tan\alpha}\left(\frac{\gamma L}{2K\tan\delta} - q\right)\cdot\left[\exp\left(-\frac{2K\tan\delta}{L}H_1\right) - \exp\left(-\frac{2K\tan\delta}{L}H\right)\right]\right\}$$
$$\cdot\left[\frac{2}{(FS - \tan\phi/\tan\alpha)\sin 2\alpha} + r_a\frac{H_1}{B} + 2r_s\frac{H - \frac{B\tan\alpha}{2}}{L}\right]^{-1}\cdot\tan(45^\circ + \phi/2) \quad (1)$$

where K is the Rankine active earth pressure coefficient, $K = \tan^2(45^\circ - \frac{\phi}{2})$; ϕ is friction the angle of backfill; δ is the friction angle of backfill–side wall interfaces, °; γ is the unit weight of backfill, kN/m^3; $H_1 = H - B\tan\alpha$, m; FS is the safety factor; $\alpha = 45^\circ + \phi/2$; r_a is the roughness of the backfill-orebody interface; and r_s is the roughness of the backfill-side wall.

3.2. Analytical Solution for CSUTB When in Contact with the NCT

Equation (1) can be used to design the required strength of backfill when in contact with the orebody. However, from Figure 3 we note that the backfill is also in contact with NCT when mining secondary stopes. In this case, Equation (1) may be too conservative to calculate the required strength due to different mechanical properties between the orebody and NCT. Backfill will be subject to a horizontal force F induced by NCT along the backwall. F is written as [27]:

$$F = \frac{1}{2}K\gamma_1 H_1^2 L \quad (2)$$

where γ_1 is the unit weight of non-cemented backfill.

The shear force S of backfill-side wall interfaces can be estimated as in [30]:

$$S = B\cdot(r_s\cdot c + \tfrac{\gamma\cdot L}{2})\cdot(H - \tfrac{B\cdot\tan\alpha}{2}) - \tfrac{B\cdot L}{2}(\tfrac{\gamma\cdot L}{2K\cdot\tan\delta} - q)$$
$$+\tfrac{L^2}{4K\cdot\tan\delta\cdot\tan\alpha}\cdot(\tfrac{\gamma\cdot L}{2K\cdot\tan\delta} - q)\cdot\left[\exp(-\tfrac{2K\cdot\tan\delta}{L}\cdot H_1) - \exp(-\tfrac{2K\cdot\tan\delta}{L}\cdot H)\right] \quad (3)$$

Considering forces equilibrium in the directions parallel and vertical to the sliding plane, FS can be obtained and evaluated as:

$$FS = \frac{cLB + (F' \cdot \cos\alpha - F \cdot \sin\alpha) \cdot \tan\phi \cdot \cos\alpha}{F' \cdot \sin\alpha \cdot \cos\alpha + F \cdot \cos^2\alpha} \tag{4}$$

where $F' = q \cdot B \cdot L + \gamma \cdot B \cdot H' \cdot L - 2S$; $H' = H - \frac{B \cdot \tan\alpha}{2}$.

Required cohesion c of backfill is written as:

$$c = \frac{(FS \cdot \sin\alpha \cdot \cos\alpha - \cos^2\alpha \cdot \tan\phi) \cdot L \cdot B \cdot p' + F \cdot \cos\alpha \cdot (FS \cdot \cos\alpha + \tan\phi \cdot \sin\alpha)}{L \cdot B + (FS \cdot \sin\alpha - \cos\alpha \cdot \tan\phi) \cdot 2 \cdot H' \cdot B \cdot r_s \cdot \cos\alpha} \tag{5}$$

The required strength of backfill when its backwall contacts with NCT can be calculated as:

$$UCS = 2 \cdot \frac{(FS \cdot \sin\alpha \cdot \cos\alpha - \cos^2\alpha \cdot \tan\phi) \cdot L \cdot B \cdot p' + F \cdot \cos\alpha (FS \cdot \cos\alpha + \tan\phi \cdot \sin\alpha)}{LB + (FS \cdot \sin\alpha - \cos\alpha \cdot \tan\phi) \cdot 2 \cdot H' \cdot B \cdot r_s \cdot \cos\alpha} \cdot \tan(45^\circ + \phi/2) \tag{6}$$

In Equations (5) and (6), p' is given as:

$$p' = \frac{L}{2K \cdot \tan\delta} \cdot \left\{ \begin{array}{l} \gamma - \frac{1}{B \cdot \tan\alpha} \cdot (\frac{\gamma \cdot L}{2K \cdot \tan\delta} - q) \cdot \\ \left[\exp(-\frac{2K \cdot \tan\delta}{L} \cdot H_1) - \exp(-\frac{2K \cdot \tan\delta}{L} \cdot H)\right] \end{array} \right\} \tag{7}$$

3.3. Required Strength Calculation

Considering different interfacial properties between backfill and adjacent stopes, required strengths of backfill can be calculated by substituting stope parameters, interface properties, and mechanical parameters of backfill into Equations (1) and (6), respectively. The related parameters are listed in Table 1; for δ, r_a and r_s, refer to [34,37]. Calculated results indicate that backfill needs a higher strength (0.82 MPa) when in contact with NCT than when in contact with the orebody (0.78 MPa). Due to the limitations stated in Section 3.1, the Mitchell model has the smallest value (0.54 MPa) and is conservative to design backfill strength.

Table 1. Inputs for required strength calculation.

L (m)	B (m)	H (m)	FS	γ (kN/m^3)	γ_1 (kN/m^3)	f (°)	δ (°)	ρ_α	ρ_σ
50	18	60	1.5	18	16.3	30	15	0.2	0.5

4. Reasonable Mix Design of CSUTB for ZGIM via Laboratory Tests

Mechanical properties, i.e., uniaxial compressive strength with different c/t ratios, solids contents, and curing ages, of CSUTB of ZGIM have been reported in a previous paper [28], and it can be noted that backfill with 1:10 c/t had a strength between 0.83 and 0.94 MPa, higher than the required strength (0.82 MPa). That is, a c/t of 1:10 could meet the strength requirement of ZGIM. Except for the strength required to keep stable when extracting adjacent stope, CSUTB also needs favorable flow characteristics to be successfully transported to underground open stopes [38]. Therefore, the main point of this laboratory test is to verify the rheological properties of CSUTB with 1:10 c/t.

4.1. Materials and Methods

4.1.1. Tailings

The tailings samples used in this study were collected from the processing plant of ZGIM. Prior to testing, tailings were mixed thoroughly to make them homogeneous. Particle size distribution, as the most significant physical characteristic of fill material of tailings, was analyzed using a Mastersizer2000 laser particle size analyzer (Malvern, Shanghai, China); the results are summarized

in Figure 5 and Table 2. Table 2 indicates that the tailings of ZGIM can be classified as super fine tailings since more than 60 wt % of the sample was finer than 20 μm and its maximum diameter is only 211 μm [39]. The portion of tailings finer than 20 μm plays an important role in paste pumpability [15].

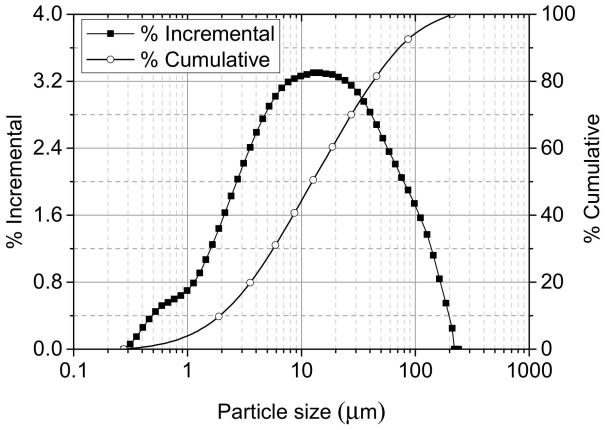

Figure 5. Particle size distribution of tailings.

Table 2. Particle size characteristics of unclassified tailings.

Characteristic Diameter	d_{10}	d_{50}	d_{60}	d_{90}	d_{100}
Size (μm)	2.17	14.2	18.7	82.9	211

Another important characteristic of tailings that needs to be identified is its chemical composition, which has a pronounced effect on the hardening process of backfill [40]. The mineralogical analysis of tailings was performed via WDX400 X-ray Fluorescence (XRF, Skyray, Suzhou, China) Spectrometer and the result is given in Table 3. The main minerals in the sample are CaO (44.41%), SiO_2 (20.91%), Fe_2O_3 (16.39%), and MgO (11.30%), indicating the high quality and activity of tailings [28].

Table 3. Chemical compositions of unclassified tailings and ordinary Portland cement (OPC) (%).

Composition	CaO	SiO_2	Fe_2O_3	MgO	Al_2O_3	SO_3	K_2O	Na_2O	TiO_2
Tailings	44.41	20.91	16.39	11.30	3.22	2.23	0.52	0.39	0.10
OPC	60.51	22.86	3.35	1.57	5.45	3.01	0.56	0.25	0.11

4.1.2. Binders and Water

Ordinary Portland cement (OPC) was chosen as the binder in this study. OPC, following the Chinese standards for "Common Portland Cement" (GB 175-2007) [41], was bought from Shenyang cement plant (Shenyang, China). The characteristics of OPC used are listed in Table 3. Tap water was used to mix the binder and tailings in the laboratory.

4.1.3. Mixture Preparation

The experimental parameters encompassed one type of c/t with four different solid contents resulting in four mixes of CSUTB. Tailings material, OPC, and water were mixed and homogenized for about 5 min in a concrete mixer. Detailed mix formulations are listed in Table 4. A high-precision electronic scale with an accuracy of 0.01 g was used to weigh ingredients.

Table 4. Summary of mix formulations of paste.

c/*t*	Solids Content
1:10	65%
1:10	68%
1:10	70%
1:10	73%

4.1.4. Slump Test

In the field, true rheological properties of pastes are not easy to obtain due to the complexity of experimental devices. Hence, the Slump test is widely used to determine the consistency of backfill due to its simplicity and convenience [42]. ASTM C143/C143M-15a [43] was followed in this study to evaluate the transportability of a fresh CSUTB mixture. Slump height is defined as the difference in height between the top of cone mold and the top of the paste after the cone has been removed. A series of slump tests were conducted in accordance with Table 4.

4.1.5. Bleeding Test

The "bleeding" phenomenon is often observed in the settlement of backfill mixture, and the bleeding rates are different with variable cement and water contents. In this test, as described in ASTM C940-16 [44], slurry was poured into a 1000 mL graduated cylinder immediately with a volume about 800 $\pm$ 10 mL after homogenized mixing. Bleeding rate was measured according to the final bleed water on the sample surface, divided by initial water volume. To evaluate the settlement behavior of mixtures, the height of bleed water at different times was recorded. Readings were taken at 5 min intervals for the first 30 min, at 10 min intervals between 30 and 60 min, and thereafter at half-hourly intervals until two successive readings showed no further bleeding. The total reading time was 150 min, while the final volume of bleeding water was measured after 24 h. Plastic film was used to cover the cylinder to prevent evaporation of the bleed water.

4.1.6. Fluidity Test

According to reported research [45–47], GB/T 2419-2005 [48] was used to study the flowability or fluidity of CSUTB mixtures. An open-ended truncated cone mold 2.4 in. (60 mm) in height with a 4 in. (100 mm) internal diameter of the upper opening and 4.8 in. (120 mm) diameter of the bottom opening was used to test the fluidity of the mix by measuring its spreading diameter. Fresh mix was poured into the mold twice, and the height of the first layer should be equal to 1.6 in. (40 mm). It is of the utmost importance that the spreading diameter of the mix should be measured immediately after the removing mold. Two measurements in directions perpendicular to each other are then carried out along the diameters. The average value of two measurements is defined as the fluidity of the mix.

4.2. Experimental Results

4.2.1. Effect of Solids Content on Slump of Fresh CSUTB with 1:10 c/t

Slump values corresponding to solids content were plotted in Figure 6 together with the relevant fitting curve. As expected, the rheological properties of CSUTB decrease with increasing solids content. The findings suggest that the slump value decreased from 288 mm (11.52 inches) to 165 mm (6.6 inches) when the solids content rose from 65% to 73%. According to [4,41,49], widely used slump values in many backfilling operations are in the range of 180 mm (7.2 inches) to 250 mm (10 inches). It can be noted that CSUTB with 73% solids content has a low slump value, meaning poor flowability during the process of transportation. As shown in Figure 6, the slump value with a certain solids content can be determined using the empirical equation obtained from polynomial regression, which is a little

different from the findings in Kesimal et al. [15]. The results of slump tests of 1:10 c/t backfill with different solids contents are also shown in Figure 7.

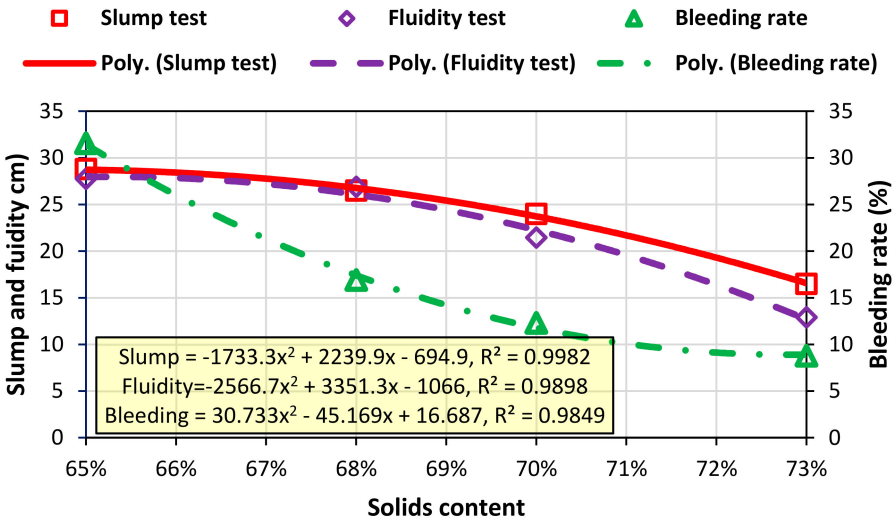

Figure 6. Slump, fluidity, and bleeding rate vs. solids content.

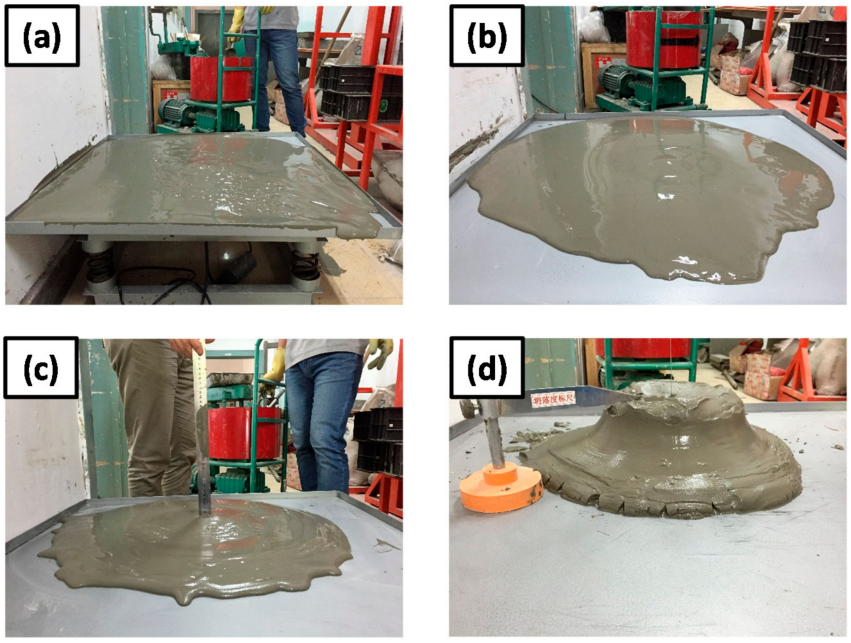

Figure 7. Slump tests of CSUTB of 1:10 c/t with different solids contents: (**a**) 65%, (**b**) 68%, (**c**) 70%, and (**d**) 73%.

4.2.2. Effect of Solids Content on Bleeding Rate of Fresh CSUTB with 1:10 c/t

As shown in Figure 6, the bleeding rate of CSUTB shows a significant decrease with higher solids content. The bleeding rates of tested CSUTBs with 1:10 c/t are 31.56% (65% solids content), 16.90% (68% solids content), 14.23% (70% solids content), and 8.79% (73% solids content), respectively. The curves of the height of bleed water, varying with settlement time, are plotted in Figure 8. It is worth noting that the solids content has a pronounced effect on the settlement speed of the CSUTB mixture. In general, a lower solids content leads to a higher bleeding speed and settles adequately

in a shorter time, e.g., the termination times of settlement are 20, 60, 80 and 60 min, respectively. The lower bleeding rate in a mixture with a higher solids content is attributed to a higher cement content. Considering the lower diameter of cement compared to tailings, the addition of cement will reduce the porosity of aggregates and contribute to a higher water retention ability. To improve the roof-contacted filling ratio and reduce underground pollution, the bleeding rate should be lower than 15% [50]. It can be concluded that the solids content should be at least 70%. There is a relationship approximate to a polynomial function between the solids content and bleeding rate, as shown in Figure 6, with a fitting correlation coefficient about 0.98.

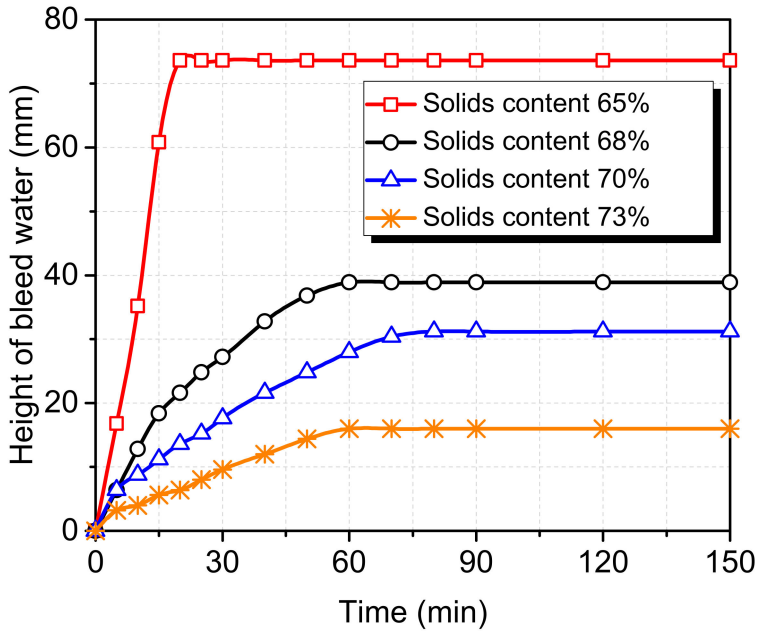

Figure 8. Natural sedimentation curves of fresh CSUTB of 1:10 c/t with different solids contents.

4.2.3. Effect of Solids Content on Fluidity of Fresh CSUTB with 1:10 c/t

Fluidity is also a common rheological index to evaluate the consistency of backfill mixture. Compared to the slump test, a fluidity test shows advantages of lower mixture consumption and easier operation [50,51]. A comparison of the fluidity of a fresh mixture with different solids contents is shown in Figure 9. It is clear from the figure that the spreading diameter and height of central accumulation horizon (CAH) obviously decreases and increases, respectively, with increasing solids content. The spreading diameter of fresh CSUTB with 65% solid content is 277.5 mm (11.1 inches) with a height of 5 mm (0.2 inches) in CAH, which means desirable transportation ability. However, when the solids content increased to 73%, the spreading diameter is only 129 mm and the height of CAH reaches 30 mm (1.2 inches), showing poor flowability. Interestingly, a segregation phenomenon was observed in a mixture with 65% solid content, as shown in Figure 9a. The segregation of backfill would make it impossible to fill the stopes entirely, leading to an unsafe work environment [52]. The fluidity, determined by spreading diameter, of mixture with 68% and 70% solids content is 269 mm (10.76 inches) and 214.5 mm (8.58 inches) respectively. In China, a fluidity value higher than 200 mm (8 inches) is often acceptable [53]. Fluidity values with regard to solids contents are illustrated in Figure 6 to produce a regressive curve. It is concluded that their relationship can be expressed by a quadratic polynomial regression equation due to a high correlation coefficient (0.99).

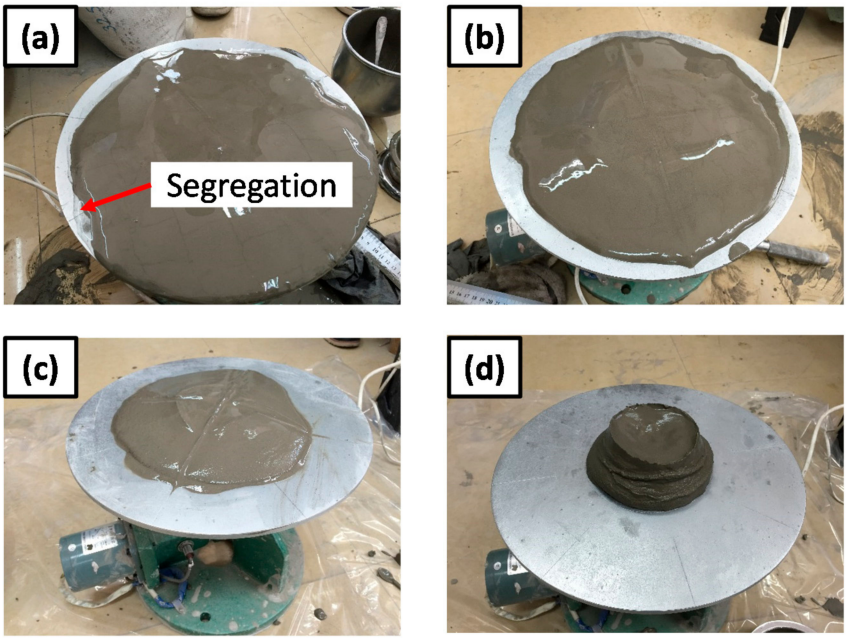

Figure 9. Slump tests of CSUTB of 1:10 c/t with different solids contents: (**a**) 65%, (**b**) 68%, (**c**) 70%, and (**d**) 73%.

4.3. Recommendation of RMP for ZGIM

After curing at 20 °C and 95% relative humidity for 28 days in a temperature- and humidity-controlled chamber, the UCS values of CSUTB with different solid contents were obtained by a uniaxial compressive test, i.e., 0.83, 0.86, 0.89 and 0.92 MPa for 65%, 68%, 70%, and 73%, respectively. According to the mechanical and rheological testing of CSUTB, an RMP with 1:10 c/t and 70% solid content is recommended for ZGIM. The reasons can be explained as following: (a) its UCS (0.89 MPa) is higher than the required strength (0.82 MPa); (b) its slump value is about 240 mm, which is in the common range of 180 to 250 mm; (c) it has an acceptable bleeding rate of 12.23%, which is lower than the limit value of 15% [50]; and (d) its fluidity is 214.5 mm, showing favorable flow characteristics [53]. That is, CSUTB with such a mix formulation can be successfully transported to underground open stopes and kept stable when mining an adjacent secondary stope due to its superior rheological and mechanical properties.

5. Numerical Modeling Studies

One of the most important reasons for using minefill technology in ZGIM is to control and relieve the subsidence to protect residential buildings and farmland. To verify the validity of the determined mix proportioning of CSUTB in subsidence control, numerical methods are suggested. Numerical methods are different from empirical methods and physical models since they can take geological and geotechnical aspects into consideration. In mining engineering, FLAC 3D (Itasca Consulting Group, Inc., Minneapolis, MN, USA), a numerical software based on the finite-difference method, is often used to analyze the ground subsidence, stress, and deformation distribution of rock and backfill [22,54–58]. Therefore, a three-dimensional model based on FLAC 3D according to the mining conditions was established for the simulation of backfill mining.

5.1. Model Geometry, Boundary, and Material Initial Conditions

A model was first built in AUTOCAD (Version 2016, Autodesk, Inc., San Rafael, CA, USA) then meshed in ANSYS (Version 16.0, ANSYS, Inc., Canonsburg, PA, USA) and thereafter imported into FLAC 3D (version 3.0) via special FISH functions. In order to minimize the boundary effect,

a significant distance from the mining area to the lateral and bottom boundary is required. Finer meshes are assigned in the domain where the orebody is located. The model dimensions were taken as 1144 m on the X-axis (EW), 50 m on the Y-axis (NS), and 755 m on the Z-axis. The reason for the small length in the Y direction (strike) is that the strike of the orebody is quite long enough relative to its width and height, which has a minor effect on the subsidence [58]. Meanwhile, the change of geometry of the orebody along the strike is not significant, which can be analyzed as a plane-strain problem [21]. Therefore, a model developed from section of No. 4–5 exploration line. The model has 199,959 zones and 38,332 nodes, as shown in Figure 10.

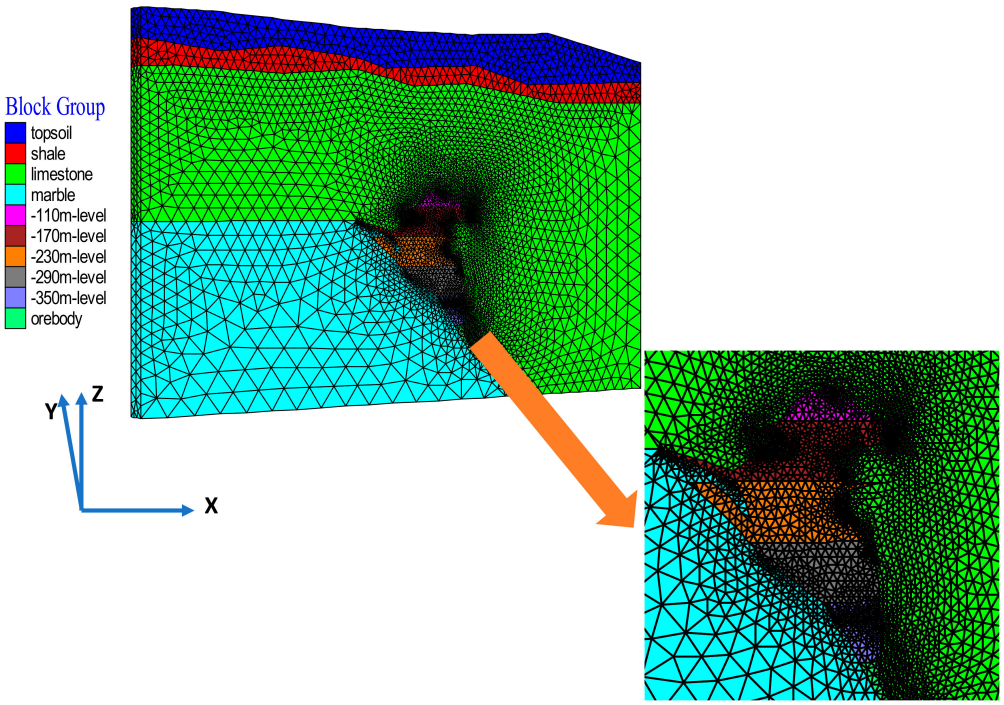

Figure 10. FLAC 3D model for backfilling mining.

The model base had been fixed laterally and vertically (pinned boundary). The lateral wall of the model had a roller boundary, meaning that movement was fixed laterally and free in the Z direction. According to the ZGIM geological report issued by the North China Engineering Investigation Institute Co., Ltd in 2007 and geostress distribution in nearby regions, regressive equations for predicting stress tensor values are given in Equation (8) and then incorporated into numerical modeling. The major principal stress is around 2.1 times the vertical stress, meaning the stress field in ZGIM is controlled by horizontal tectonic stress rather than self-weighted stress.

$$\begin{cases} \sigma_{h,\max} = 1.934 + 0.0478H \text{ (MPa)} \\ \sigma_{h,\min} = 0.409 + 0.0292H \text{ (MPa)} \\ \sigma_v = 0.485 + 0.0272H \text{ (MPa)} \end{cases} \quad (8)$$

where $\sigma_{h,\max}$, $\sigma_{h,\min}$, and σ_v are the maximum principal, minimum principal, and vertical principal stresses; H is the buried depth. Orientation of maximum horizontal principal stress is approximately NW in accord with the orientation of the maximum tectonic stress.

5.2. Constitutive Model and Material Properties

One of the most significant parts of numerical modeling is assigning the constitutive model, which describes the mechanical behavior including yielding and post-crack of geomaterial [56]. In FLAC3D, elastic, strain softening, and Mohr-coulomb (*mohr*) models are often used for mining engineering. In this simulation, the *mohr* model is used to simulate the behavior of rock and backfill, while the elastic model is used for quaternary topsoil. Mechanical properties of different materials simulated in this study are given in Table 5, based on laboratory tests and field investigation. Backfill tensile strength was evaluated by the split tensile strength of CSUTB with 1:10 c/t and 70% solid content after 28-day curing. Internal friction angle and cohesion of CSUTB with that mix design are obtained from backfilling technical report of ZGIM [59].

Table 5. Input parameters for FLAC 3D model.

Type	Density ($g \cdot m^{-3}$)	Tensile Strength (MPa)	Cohesion (MPa)	Internal Frictional Angle (°)	Elastic Modulus (GPa)	Poisson's Ratio
quaternary topsoil	2.20	-	0.1	-	3.20	0.32
Shale	2.62	1.55	6.45	34	6.30	0.31
crystalline limestone	2.67	1.60	5.28	46	8.23	0.27
Orebody	3.95	1.53	6.25	34	6.30	0.31
Marble	2.78	1.65	5.72	45	8.30	0.30
CSUTB (1:10 c/t)	1.80	0.47	0.73	33	0.93	0.24

5.3. Numerical Modeling Results

After generating the numerical model, initializing the mechanical parameters, and fixing the boundaries, the model was first solved as an elastic model for the equilibrium state. The mining and backfilling sequences of levels discussed earlier were then followed. In this study, the effect of blast was not taken into consideration and the model was analyzed under static loading. The rock, orebody, and backfill were subjected to *mohr* failure criteria. A total of 60 monitoring points in the central line of upper surface along the X direction were set for recording ground subsidence after each extraction.

5.3.1. Subsidence Parameters

To evaluate the ground subsidence, five deformation parameters, i.e., VD, HD, HDR, curvature, and inclination, were introduced. VD is the vertical deformation of a monitoring point, which means ascent in positive and descent in negative. The VD is expressed as:

$$VD = V_{n'} - V_n \tag{9}$$

where $V_{n'}$ is the elevation of the monitoring point after mining, mm; V_n is the elevation of the monitoring point before mining, mm.

HD is the horizontal component of a displacement vector for monitoring points. In the orebody strike section, HD is positive when monitoring points shift to the right, and negative when they shift to the left. HD is written as:

$$HD = H_{n'} - H_n \tag{10}$$

where $H_{n'}$ and H_n are the distances from the monitoring point to the control point after and before extraction, respectively, in mm.

Inclination is the ratio of the VD difference to the horizontal distance between two adjacent monitoring points. Ground subsidence often leads to leaning of buildings, which has a significant influence on their stability and stress state. Incline (i_{AB}) is evaluated as:

$$i = \frac{\Delta VD}{\Delta H} \tag{11}$$

where i_{AB} is the incline, mm/m; ΔVD and ΔH are the VD difference (in millimeters) and the horizontal distance (in meters) between two adjacent monitoring points, respectively.

Curvature K is the ratio of the incline difference to the midpoint distance between two adjacent line segments, which makes the surface crooked. Then, the force balance between the earth and the foundations of buildings would be destroyed, causing deformation and destruction of the buildings. The style of cracks in buildings is associated with the positive-negative values of curvature. K is expressed as:

$$K = \frac{\Delta i}{1/2\Delta H_{mid}} \tag{12}$$

where K is the curvature, 10^{-3}/m; Δi (mm/m) and ΔH_{mid} (m) are the incline difference and midpoint distance between two adjacent line segments, respectively.

HDR is the horizontal deformation rate of the ground surface, which is equal to the ratio of HD difference to the horizontal distance between two adjacent monitoring points. Buildings in China are mainly made of brick and concrete, showing high compressive capacity and low tensile ability. Therefore, a small HDR could cause cracks at the weak parts of buildings, leading to fracture failure. HDR is determined as:

$$HDR = \frac{\Delta HD}{\Delta H} \tag{13}$$

where HDR, mm/m; ΔHD (mm); and ΔH (m) are different horizontal distances between two adjacent monitoring points.

5.3.2. Subsidence Analysis

As discussed earlier, the mining sequence of five levels in ZGIM is as follows: −350 m level > −290 m level > −230 m level > −170 m level > −110 m level. After each extraction, the subsidence data were recorded, as shown in Table 6 and Figure 11. It can be noted from Figure 11 that subsidence increases significantly with increasing extraction area. The vertical deformation (VD) value of monitoring points increases closer to the mining center, which leads to a V-shaped settlement area. It is worth observing that the maximum horizontal deformation (HD) and incline occur at the bilateral parts of the mining center with a distance about 200 m. In the mining center, the HD is nearly zero but the HD rate is maximum, meaning buildings may occur some cracks caused by tensile stress. The maximum HD area shows the highest inclination but the lowest HD rate, which commonly makes a building unstable due to the deviation from the center of gravity. From Figure 11b, we can find the maximum subsidence point moves to the left as the extraction activity continues, which is associated with an irregular shape of the orebody and ascending mining sequence. This finding is also consistent with the findings in [26]. Please note the value of subsidence parameters after mining the −110 m level are nearly the same as extraction of the −170 m level.

Table 6. Maximum deformation values with mining sequence (absolute value).

Levels	Vertical Deformation (mm)	Horizontal Deformation (mm)	Inclination (mm/m)	Curvature (10^{-3}/m)	Horizontal Deformation Rate (mm/m)
−350	16.914	4.671	0.0294	0.000224	0.0305
−290	77.017	21.083	0.1500	0.001258	0.1893
−230	164.68	55.747	0.3661	0.003009	0.4157
−170	222.32	78.085	0.5306	0.004857	0.5106
−110	225.04	79.370	0.5368	0.004890	0.5172

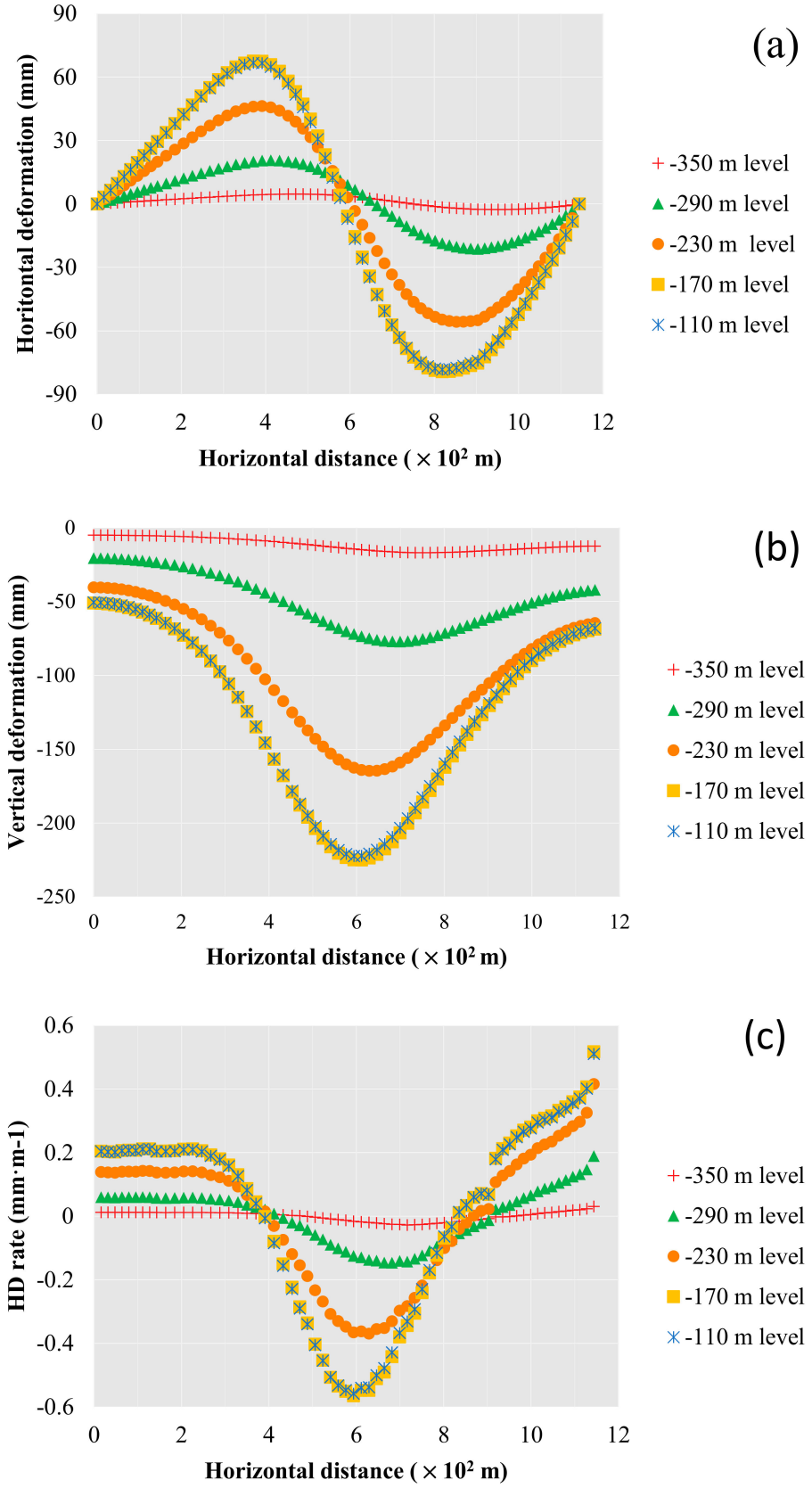

Figure 11. *Cont.*

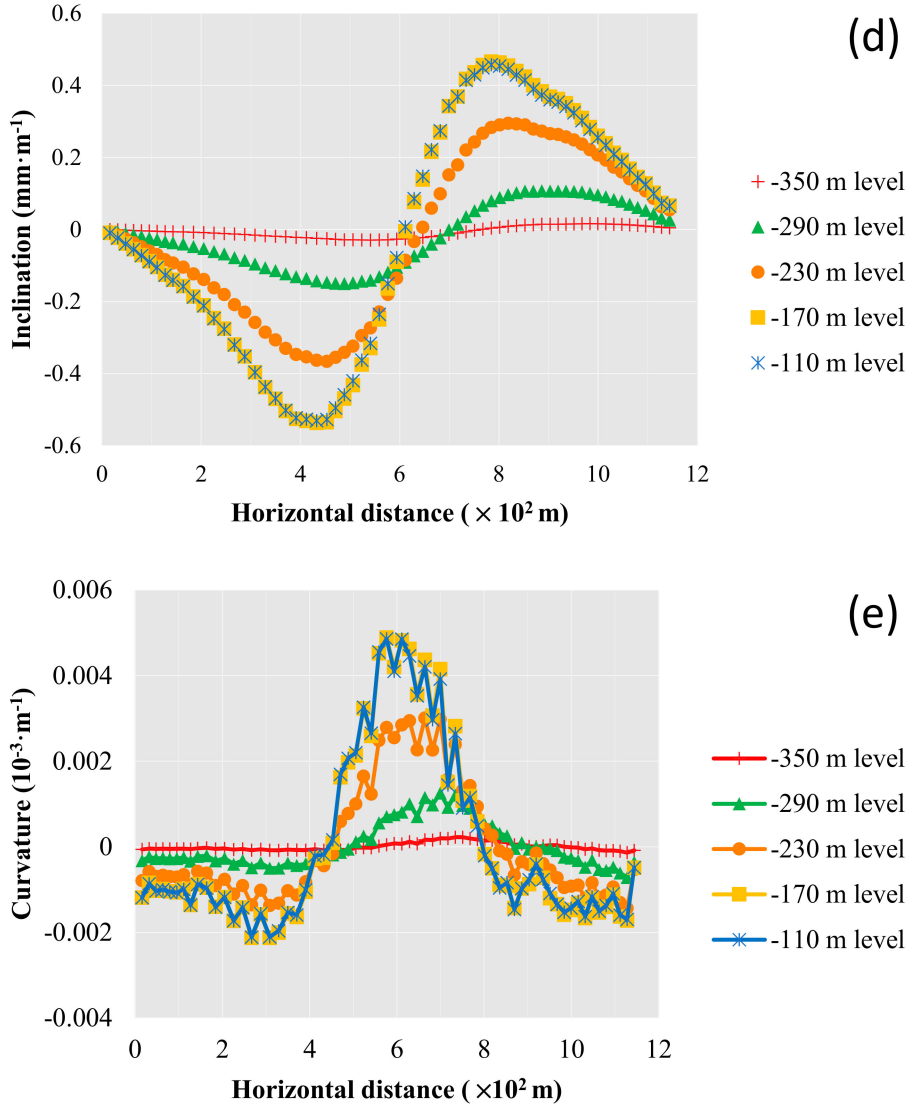

Figure 11. Deformation distribution after extracting each level. (**a**) Horizontal deformation; (**b**) Vertical deformation; (**c**) Horizontal deformation rate; (**d**) Inclination; (**e**) Curvature.

As shown in Table 6, the deformation values were quite small when the −350 m level was mined first. However, the VD, HD, HD rate, curvature, and incline after extracting the −110 m level were 13.30, 16.99, 16.96, 21.83, and 18.26 times, respectively, the values of extraction of −350 m. A significant increase in deformation values was found after mining the −230 m level, which can be explained by it having the highest ore reserve. The allowable deformation values of ZGIM ground according to GB-50771-2012 [60] are ±6 mm/m HD rate, ±4 mm/m inclination, and $\pm 0.4 \times 10^{-3}$ m^{-1} curvature. Compared with limited values, the final deformation values of ZGIM (0.5172 mm/m, 0.5368 mm/m, and 0.004890×10^{-3} m^{-1}) are small and safe. Therefore, it can be concluded that subsidence in ZGIM is acceptable and will not cause obvious damage to the villages and farmland above the mining area; and the backfill mining method can ensure the ground deformation in a controllable range. Moreover, the recommended mix proportioning of CSUTB is reasonable and valid.

6. Conclusions

A study of the use of cemented super-fine tailings backfill in an underground iron mine for the control of subsidence has been presented. An analytical solution (for determining required strength)

and laboratory tests (for evaluating mechanical and rheological properties) have been investigated to determine the optimal mix of CSUTB for ZGIM. Where necessary, a 3D numerical model incorporating realistic mining sequences has been used to verify the validity of CSUTB with RMP in subsidence control. The conclusions based on the results are as follows:

(1) The present study proposes an modified analytical solution for evaluating the required strength of backfill when in contact with NCT based on Li [30], which then is used in a case study. The required strength of backfill for ZGIM is 0.82 and 0.78 MPa when in contact with the NCT and orebody, respectively.
(2) The results indicate that the rheological properties of CSUTB decrease with increasing solid contents. The rheology, i.e., slump, fluidity, and bleeding rate values, with a certain solid content, can be determined by empirical quadratic polynomial regression equations.
(3) Based on mechanical and rheological testing on CSUTB, a reasonable mix of 1:10 c/t with 70% solid content is recommended for ZGIM. CSUTB with such proportions can meet the strength and transportation requirements as the same time.
(4) According to the results of numerical modeling, the maximum vertical and horizontal deformation after extracting −110 m level are 225.04 and 79.370 mm, respectively. The subsidence will increase significantly after mining the −230 m level due to having the largest iron reserves. However, the change of deformation is not clear between extraction at the −110 and −170 m levels. The surface subsidence weighs more toward to left side due to irregular geometry of orebody.
(5) The maximum inclination (0.5368 mm/m), curvature (0.004890×10^{-3}/m), and horizontal deformation rate (0.5172 mm/m) are sufficiently small compared with critical values (4 mm/m, 0.4×10^{-3} m^{-1} and 6mm/m, respectively), which means the subsidence caused by mining activities will not influence the safety of residential buildings and farmland. The results also indicate that the recommended formulation of ZGIM is reasonable and valid.

The influence of mining sequence and backfill properties on surface subsidence should be further investigated. Meanwhile, future study should also focus on the substitution of fly ash or blast furnace slag for cement to reduce the backfill cost.

Acknowledgments: The authors acknowledge financial support from the National Natural Science foundation of China (No. 51774066).

Author Contributions: Shiqiang Hu and Hao Li designed and performed the experiments; Songbo Li collected and archived the experiment results; Lei Yang and Jingping Qiu analyzed the experimental data and initiated the writing of the paper; Haiqiang Jiang proofread the manuscript.

Conflicts of Interest: The authors declare no conflict of interest.

Abbreviations

CPB	cemented paste backfill
CSUTB	cemented super-fine unclassified tailings backfill
ZGIM	Zhongguan Irom Mine
UCS	uniaxial compressive strength
NCT	non-cemented tailings
RMP	reasonable mix proportion
c/t	cement to tailings
OPC	ordinary Portland cement
mohr	Mohr–coulomb
VD	vertical deformation
HD	horizontal deformation
HDR	horizontal deformation rate
CAH	central accumulation horizon
SFT	super-fine tailings

References

1. Fall, M.; Célestin, J.C.; Pokharel, M.; Touré, M. A contribution to understanding the effects of curing temperature on the mechanical properties of mine cemented tailings backfill. *Eng. Geol.* **2010**, *114*, 397–413. [CrossRef]
2. Nasir, O.; Fall, M. Modeling the heat development in hydrating CPB structures. *Comput. Geotech.* **2009**, *36*, 1207–1218. [CrossRef]
3. Sun, W.; Wu, A.; Hou, K.; Yang, Y.; Liu, L.; Wen, Y. Real-time observation of meso-fracture process in backfill body during mine subsidence using X-ray CT under uniaxial compressive conditions. *Constr. Build. Mater.* **2016**, *113*, 153–162. [CrossRef]
4. Jiang, H.; Fall, M.; Cui, L. Freezing behaviour of cemented paste backfill material in column experiments. *Constr. Build. Mater.* **2017**, *147*, 837–846. [CrossRef]
5. Yin, S.; Wu, A.; Hu, K.; Wang, Y.; Zhang, Y. The effect of solid components on the rheological and mechanical properties of cemented paste backfill. *Miner. Eng.* **2012**, *35*, 61–66. [CrossRef]
6. Benzaazoua, M.; Bussière, B.; Demers, I.; Aubertin, M.; Fried, É.; Blier, A. Integrated mine tailings management by combining environmental desulphurization and cemented paste backfill: Application to mine Doyon, Quebec, Canada. *Miner. Eng.* **2008**, *21*, 330–340. [CrossRef]
7. Fall, M.; Pokharel, M. Coupled effects of sulphate and temperature on the strength development of cemented tailings backfills: Portland cement-paste backfill. *Cem. Concr. Composit.* **2010**, *32*, 819–828. [CrossRef]
8. Sivakugan, N.; Rankine, R.M.; Rankine, K.J.; Rankine, K.S. Geotechnical considerations in mine backfilling in Australia. *J. Clean. Prod.* **2006**, *14*, 1168–1175. [CrossRef]
9. Liang, C.; Fall, M. An evolutive elasto-plastic model for cemented paste backfill. *Comput. Geotech.* **2016**, *71*, 19–29.
10. Yilmaz, E.; Belem, T.; Benzaazoua, M. Specimen size effect on strength behavior of cemented paste backfills subjected to different placement conditions. *Eng. Geol.* **2015**, *185*, 52–62. [CrossRef]
11. Ouellet, S.; Bussière, B.; Aubertin, M.; Benzaazoua, M. Microstructural evolution of cemented paste backfill: Mercury intrusion porosimetry test results. *Cem. Concr. Res.* **2007**, *37*, 1654–1665. [CrossRef]
12. Doherty, J.P. A numerical study into factors affecting stress and pore pressure in free draining mine stopes. *Comput. Geotech.* **2015**, *63*, 331–341. [CrossRef]
13. Ke, X.; Hou, H.; Zhou, M.; Wang, Y.; Zhou, X. Effect of particle gradation on properties of fresh and hardened cemented paste backfill. *Constr. Build. Mater.* **2015**, *96*, 378–382. [CrossRef]
14. Liang, C.; Fall, M. Mechanical and thermal properties of cemented tailings materials at early ages: Influence of initial temperature, curing stress and drainage conditions. *Constr. Build. Mater.* **2016**, *125*, 553–563.
15. Kesimal, A.; Yilmaz, E.; Ercikdi, B. Evaluation of paste backfill mixtures consisting of sulphide-rich mill tailings and varying cement contents. *Cem. Concr. Res.* **2004**, *34*, 1817–1822. [CrossRef]
16. Deng, D.Q.; Liu, L.; Yao, Z.L.; Song, K.I.; Lao, D.Z. A practice of ultra-fine tailings disposal as filling material in a gold mine. *J. Environ. Manag.* **2017**, *196*, 100–109. [CrossRef] [PubMed]
17. Amaratunga, L.M.; Yaschyshyn, D.N. Development of a high modulus paste fill using fine gold mill tailings. *Geotech. Geol. Eng.* **1997**, *15*, 205–219. [CrossRef]
18. Kesimal, A.; Ercikdi, B.; Yilmaz, E. The effect of desliming by sedimentation on paste backfill performance. *Miner. Eng.* **2003**, *16*, 1009–1011. [CrossRef]
19. Fall, M.; Benzaazoua, M.; Ouellet, S. Experimental characterization of the influence of tailings fineness and density on the quality of cemented paste backfill. *Miner. Eng.* **2005**, *18*, 41–44. [CrossRef]
20. Ke, X.; Zhou, X.; Wang, X.; Wang, T.; Hou, H.; Zhou, M. Effect of tailings fineness on the pore structure development of cemented paste backfill. *Constr. Build. Mater.* **2016**, *126*, 345–350. [CrossRef]
21. Siriwardane, H.J.; Kannan, R.S.; Ziemkiewicz, P.F. Use of waste materials for control of acid mine drainage and subsidence. *J. Environ. Eng.* **2003**, *129*, 910–915. [CrossRef]
22. Zhu, X.J.; Guo, G.L.; Fang, Q. Coupled discrete element-finite difference method for analyzing subsidence control in fully mechanized solid backfilling mining. *Environ. Earth Sci.* **2016**, *75*, 683. [CrossRef]
23. Zhang, J.; Zhang, Q.; Sun, Q.; Gao, R.; Germain, D.; Abro, S. Surface subsidence control theory and application to backfill coal mining technology. *Environ. Earth Sci.* **2015**, *74*, 1439–1448. [CrossRef]
24. Guo, G.L.; Zhu, X.J.; Zha, J.F.; Wang, Q. Subsidence prediction method based on equivalent mining height theory for solid backfilling mining. *Trans. Nonferr. Met. Soc. China* **2014**, *24*, 3302–3308. [CrossRef]

25. Sui, W.; Zhang, D.; Cui, Z.C.; Wu, Z.; Zhao, Q. Environmental implications of mitigating overburden failure and subsidences using paste-like backfill mining: A case study. *Int. J. Min. Reclam. Environ.* **2015**, *29*, 521–543. [CrossRef]
26. Huang, G.; Kulatilake, P.H.; Shreedharan, S.; Cai, S.; Song, H. 3-D discontinuum numerical modeling of subsidence incorporating ore extraction and backfilling operations in an underground iron mine in China. *Int. J. Min. Sci. Technol.* **2017**, *27*, 191–201. [CrossRef]
27. Yang, Z.; Zhai, S.; Gao, Q.; Li, M. Stability analysis of large-scale stope using stage subsequent filling mining method in Sijiaying iron mine. *J. Rock Mech. Geotech. Eng.* **2015**, *7*, 87–94. [CrossRef]
28. Qiu, J.; Yang, L.; Sun, X.; Xing, J.; Li, S. Strength characteristics and failure mechanism of cemented super-fine unclassified tailings backfill. *Minerals* **2017**, *7*, 58. [CrossRef]
29. Li, L.; Aubertin, M. A modified solution to assess the required strength of exposed backfill in mine stopes. *Can. Geotech. J.* **2012**, *49*, 994–1002. [CrossRef]
30. Li, L. Generalized Solution for Mining Backfill Design. *Int. J. Geomech.* **2014**, *14*, 04014006. [CrossRef]
31. Li, L. Analytical solution for determining the required strength of a side-exposed mine backfill containing a plug. *Can. Geotech. J.* **2013**, *51*, 508–519. [CrossRef]
32. Li, L.; Aubertin, M. An improved method to assess the required strength of cemented backfill in underground stopes with an open face. *Int. J. Min. Sci. Technol.* **2014**, *24*, 549–558. [CrossRef]
33. Liu, Z.X.; Ming, L.; Xiao, S.Y.; Guo, H.Q. Damage failure of cemented backfill and its reasonable match with rock mass. *Trans. Nonferr. Met. Soc. China* **2015**, *25*, 954–959. [CrossRef]
34. Yang, P.; Li, L.; Aubertin, M. A new solution to assess the required strength of mine backfill with a vertical exposure. *Int. J. Geomech.* **2017**, *17*. [CrossRef]
35. Mitchell, R.J.; Olsen, R.S.; Smith, J.D. Model studies on cemented tailings used in mine backfill. *Can. Geotech. J.* **1982**, *19*, 14–28. [CrossRef]
36. Fall, M.; Nasir, O. Mechanical Behaviour of the Interface Between Cemented Tailings Backfill and Retaining Structures Under Shear Loads. *Geotech. Geol. Eng.* **2010**, *28*, 779–790. [CrossRef]
37. Liu, G.; Li, L.; Yang, X.; Guo, L. Numerical analysis of stress distribution in backfilled stopes considering interfaces between the backfill and rock walls. *Int. J. Geomech.* **2017**, *17*. [CrossRef]
38. Ouattara, D.; Yahia, A.; Mbonimpa, M.; Belem, T. Effects of superplasticizer on rheological properties of cemented paste backfills. *Int. J. Miner. Process.* **2017**, *161*, 28–40. [CrossRef]
39. Ercikdi, B.; Cihangir, F.; Kesimal, A.; Deveci, H.; Alp, İ. Utilization of water-reducing admixtures in cemented paste backfill of sulphide-rich mill tailings. *J. Hazard. Mater.* **2010**, *179*, 940–946. [CrossRef] [PubMed]
40. Benzaazoua, M.; Fall, M.; Belem, T. A contribution to understanding the hardening process of cemented pastefill. *Miner. Eng.* **2004**, *17*, 141–152. [CrossRef]
41. *Common Portland Cement*; Chinese Standard GB 175-2007; Standardization Administration of China: Beijing, China, 2007.
42. Belem, T.; Benzaazoua, M. Design and application of underground mine paste backfill technology. *Geotech. Geol. Eng.* **2008**, *26*, 147–174. [CrossRef]
43. *Standard Test Method for Slump of Hydraulic-Cement Concrete*; ASTM C143/C143M-15a; ASTM International: West Conshohocken, PA, USA, 2015.
44. *Standard Test Method for Expansion and Bleeding of Freshly Mixed Grouts for Preplaced-Aggregate Concrete in the Laboratory*; ASTM C940–16; ASTM International: West Conshohocken, PA, USA, 2016.
45. Meng, T.; Yu, Y.; Qian, X.; Zhan, S.; Qian, K. Effect of nano-TiO_2 on the mechanical properties of cement mortar. *Constr. Build. Mater.* **2012**, *29*, 241–245. [CrossRef]
46. Ouyang, X.; Guo, Y.; Qiu, X. The feasibility of synthetic surfactant as an air entraining agent for the cement matrix. *Constr. Build. Mater.* **2008**, *22*, 1774–1779. [CrossRef]
47. Li, C.; Sun, H.; Yi, Z.; Li, L. Innovative methodology for comprehensive utilization of iron ore tailings: Part 2: The residues after iron recovery from iron ore tailings to prepare cementitious material. *J. Hazard. Mater.* **2010**, *174*, 78–83. [CrossRef] [PubMed]
48. *Test Method for Fluidity of Cement Mortar*; Chinese Standards GB/T 2419-2005; Standardization Administration of China: Beijing, China, 2005.
49. Ghirian, A.; Fall, M. Coupled thermo-hydro-mechanical–chemical behaviour of cemented paste backfill in column experiments. Part I: Physical, hydraulic and thermal processes and characteristics. *Eng. Geol.* **2013**, *164*, 195–207. [CrossRef]

50. Yang, L.; Wang, J.; Qiu, J.; Xing, J.; Sun, X. Ratio optimization of unclassified tailings cemented backfill material based on orthogonal experiment. *Conserv. Util. Miner. Resour.* **2017**, *3*, 21–25. (In Chinese)
51. Yao, Y.; Sun, H. A novel silica alumina-based backfill material composed of coal refuse and fly ash. *J. Hazard. Mater.* **2012**, *213*, 71–82. [CrossRef] [PubMed]
52. Ercikdi, B.; Cihangir, F.; Kesimal, A.; Deveci, H. Practical Importance of Tailings for Cemented Paste Backfill. In *Paste Tailings Management*; Springer International Publishing: Cham, Switzerland, 2017; pp. 7–32.
53. Zhang, J.W.; Ni, W.; Hu, W.; Huang, X.Y. Research on the Fluidity of Backfilling Material with Preparation of Steel Slag Gel System. *Met. Mine* **2013**, *5*, 153–156.
54. Nasir, O.; Fall, M. Coupling binder hydration, temperature and compressive strength development of underground cemented paste backfill at early ages. *Tunn. Undergr. Space Technol.* **2010**, *25*, 9–20. [CrossRef]
55. Li, L.; Aubertin, M. Numerical investigation of the stress state in inclined backfilled stopes. *Int. J. Geomech.* **2009**, *9*, 52–62. [CrossRef]
56. Salmi, E.F.; Nazem, M.; Karakus, M. The effect of rock mass gradual deterioration on the mechanism of post-mining subsidence over shallow abandoned coal mines. *Int. J. Rock Mech. Min. Sci.* **2017**, *91*, 59–71. [CrossRef]
57. Hassani, F.; Mortazavi, A.; Shabani, M. An investigation of mechanisms involved in backfill-rock mass behaviour in narrow vein mining. *J. South. Afr. Inst. Min. Metall.* **2008**, *108*, 463–472.
58. Corkum, A.G.; Board, M.P. Numerical analysis of longwall mining layout for a Wyoming Trona mine. *Int. J. Rock Mech. Min. Sci.* **2016**, *89*, 94–108. [CrossRef]
59. *Backfilling Technical Report of Zhongguan Iron Mine*; North China University of Science and Technology: Tangshan, China, 2016.
60. *China National Standards, Code for Design of Nonferrous Metal Mining*; Chinese Standards GB-50771-2012; Standardization Administration of China: Beijing, China, 2012.